# PROCEEDINGS OF SPIE

SPIEDigitalLibrary.org/conference-proceedings-of-spie

An implementation of data assimilation techniques for transmural visualization of action potential propagation in cardiac tissue

Beam, Christopher, Linte, Cristian, Otani, Niels

Christopher Beam, Cristian Linte, Niels F. Otani, "An implementation of data assimilation techniques for transmural visualization of action potential propagation in cardiac tissue," Proc. SPIE 11317, Medical Imaging 2020: Biomedical Applications in Molecular, Structural, and Functional Imaging, 113171L (5 March 2020); doi: 10.1117/12.2550467



Event: SPIE Medical Imaging, 2020, Houston, Texas, United States

# An Implementation of Data Assimilation Techniques for Transmural Visualization of Action Potential Propagation in Cardiac Tissue

Christopher Beam<sup>a</sup>, Cristian Linte<sup>b,c</sup>, and Niels Otani<sup>a</sup>

<sup>a</sup>School of Mathematical Science, Rochester Institute of Technology, Rochester, NY, USA
 <sup>b</sup>Center for Imaging Science, Rochester Institute of Technology, Rochester, NY, USA
 <sup>c</sup>Biomedical Engineering, Rochester Institute of Technology, Rochester, NY, USA

#### ABSTRACT

A number of models have been put forward which describe the motion and propagation of action potentials within cardiac muscle tissue. The information produced by these models can be unverifiable, as no techniques currently exist to accurately measure voltage within the walls of the cardiac tissue, especially in an *in vivo* environment. In most situations it is much simpler to measure the contractile motion of the cardiac muscle, which is one of the results of the propagation of these action potentials. Prior work has suggested that one can solve an inverse problem to derive the action potentials present in the cardiac tissue from measurements of the displacement caused by the contractile motion; nevertheless, the solutions to this inverse problem degrade quickly in the face of error in the measurements of these displacements. In our work, we show that one potential solution for reducing the effects of these errors is through the implementation of the Unscented Kalman Filter. This technique allows us to assimilate our error-prone measurements with knowledge of an electrophysiological model to improve our estimates and help refine our solutions to the inverse problem. Using this process, we are able to solve the one dimensional problem in a way that reduces the error present in our estimates significantly, which, in turn, allows us to more accurately resolve the electrical behavior in our system.

## 1. INTRODUCTION

A number of mathematical models have been derived which describe the propagation of electrical Action Potentials (APs) in cardiac tissue. However, current medical technology does not allow us to accurately measure the large-scale activity associated with this propagation. Clinically, we rely on diagnostic tools such as the electrocardiogram (ECG) and electrophysiology (EP) studies to provide us with some information about the heart's state. While useful, these tests do not provide us with information concerning the fundamental dynamics that dictates a patient's cardiac rhythm. The incompleteness of the data gathered prevents us from making claims with certainty. For instance, it is strongly suspected that ventricular fibrillation (VF) is caused by re-entrant AP waves, however without an accurate method for measuring the AP waves in a clinical setting, we have no way to be sure, as the nature of the waves' dynamics is controversial.<sup>1</sup>

Various techniques have been developed to overcome this deficiency. These techniques could be used to determine patterns which exist during VF and other abnormal rhythms. Rudy  $et\ al.^{2,3}$  and others have developed ECGi techniques that allow the tracking of AP propagation from electrodes on the body surface, but this technique cannot yet provide transmural information. Plunge electrodes can only give information at a very low spatial resolution and introduce heterogeneities which can influence AP propagation  $^{4,5,6,7}$ . Transillumination and optical tomography are both promising, but rely on voltage-sensitive dyes which are phototoxic, preventing their use  $in\ vivo$ .

Our work follows from that of Otani, et al., 11 which proposes the use of magnetic resonance imaging, computed tomography or ultrasound to non-invasively track the full 3D contractile motion resulting from the electrical

Further author information: (Send correspondence to Christopher Beam)

Christopher Beam: E-mail: cbb7953@rit.edu Critian A. Linte: E-mail: calbme@rit.edu Niels Otani: E-mail:nfosma@rit.edu

Medical Imaging 2020: Biomedical Applications in Molecular, Structural, and Functional Imaging, edited by Andrzej Krol, Barjor S. Gimi, Proc. of SPIE Vol. 11317, 113171L ⋅ © 2020 SPIE ⋅ CCC code: 1605-7422/20/\$21 ⋅ doi: 10.1117/12.2550467

activity in the cardiac muscle. These techniques allow for high spatial resolution and, for ultrasound, high temporal resolution necessary to visualize fast, non-repeating events<sup>12</sup>, <sup>13</sup> Using the model presented in Otani et al. <sup>11</sup>'s work, we are able to solve the inverse problem associated with this system; that is, solving for the active, voltage-induced stresses from known displacements. However, their work found that the model only worked well to solve this problem when the displacements were sufficiently accurate. The presence of uncertainty causes the solution to this inverse problem to become unreliable. The work of Wang, et al. <sup>14</sup> attempts to solve a similar problem to this one. However their work focuses on reconstructing electrophysiological data from indirect body-surface electrical measurements, while our work intends to reconstruct this electrophysiological data from direct measurements of tissue displacement

Here we report our results from the application of one method for the reduction of the influence of this noise, namely the implementation of the Unscented Kalman Filter <sup>15,16,17</sup> as a state-estimation tool. Utilizing the Otani, et al. model in conjunction with the FitzHugh-Nagumo<sup>18,19</sup> model of AP propagation, we have successfully applied the Unscented Kalman Filter as a tool to improve the estimations associated with the solution of the inverse problem in the face of uncertain measurements of tissue displacements. We have implemented this solution in a one-dimensional "cable" geometry as a simplified model of cardiac fiber behavior, so that we may study the reconstruction of the active stresses generated in the fiber that give rise to the measured deformations.

#### 2. METHODS

#### 2.1 Cardiac Mechanical Model

We begin with the same linearized stress-strain relationship employed in the Otani et al. study::

$$\frac{\partial}{\partial X_N} \left[ \frac{1}{2} \frac{\partial T_{NM}}{\partial E_{PQ}} (0) \left( \frac{\partial \delta x_P}{\partial X_Q} + \frac{\partial \delta x_Q}{\partial X_P} \right) + T_{NM}^{active} - p \delta_{NM} \right] = 0 \tag{1}$$

$$\frac{\partial \delta x_M}{\partial x_M} = 0 \tag{2}$$

Here,  $X_N$  represents the coordinates in the undeformed coordinate system,  $T_{MN}$  is the passive second Piola-Kirchoff stress tensor,  $E_{PQ}$  is the Lagrange-Green strain tensor, p is the local hydrostatic pressure,  $T_{NM}^{active}$  is the active second Piola-Kirchoff stress tensor due to the force induced by the action potentials, and  $\delta x_P$  represent the local displacements. The indices M, N, P, Q span the values 1, 2, and 3, representing the 3 spatial dimensions.

First, in an effort to simplify computation, we will be examining the one-dimensional version of the model:

$$\frac{\partial}{\partial x} \left( k \frac{\partial \delta x}{\partial x} + T^{active} \right) = 0 \tag{3}$$

This equation is essentially an application of Hooke's Law for springs. Note that, in 1D formulation, we no longer have a pressure term, as pressure is strictly a higher-dimensional phenomenon, and the Piola-Kirchoff stress tensor is replaced at this time with a constant, k. We can linearize this model as follows using a simple finite element discretization:

$$C\vec{\delta x} = -B\vec{T}^{active} \tag{4}$$

We then define the matrix  $A = C^+B$ , where  $C^+$  is the pseudoinverse of C. This matrix allows us to solve the forward problem  $\delta \vec{x} = A \vec{T}^{active}$  and to attempt to solve the inverse problem  $A^+ \delta \vec{x} = \vec{T}^{active}$  in a least-squares sense.

The forward problem described in Equation 4 is easily solved given some known active stress. And, in the event of no uncertainty, the least-squares solution to the inverse problem associated with this equation is also easily accomplished to working precision. However, in the presence of random noise or uncertainty afflicting our knowledge of the displacement, our naive least-squares solutions to the inverse problem quickly degrade and become entirely unreliable. To that end, we have utilized the Kalman Filter to improve our attempts at solving the inverse problem by also ascribing dynamics to the system.

# 2.2 Cardiac Electrical Dynamics

For these initial tests of our techniques, we have chosen to utilize the FitzHugh-Nagumo (FHN) model of cardiac electrical dynamics. This model utilizes a pair of coupled dynamical equations which describe the membrane potential difference between the inside and outside of the cell, in addition to a variable which describes how the cell recovers from the sudden change in membrane potential associated with a passing AP. The equations associated with this model are as follows:

$$\frac{\partial v}{\partial t} = \Delta v + \frac{1}{\epsilon} (v - \frac{v^3}{3} - w)$$
$$\frac{\partial w}{\partial t} = \epsilon (v - \gamma w + \beta)$$

Here, the dynamical variable v represents the membrane potential at any point in space and time within the domain, w is a variable representing the recovery of the tissue from the heightened membrane potential, v.  $\Delta$  represents the Laplacian, and  $\beta$ ,  $\gamma$  and  $\epsilon$  are constants. With this pair of equations and appropriate initial conditions, we are able to simulate an AP wave passing from one end of the domain to the other. More complicated dynamics are also possible, including spiral and scroll waves, but we have not attempted to implement these dynamics at this time. Additionally, for the purposes of modeling the mechanics, we have made the assumption that  $v = T^{active}$ . This assumption is inaccurate, but it allows us to constrain our model to a reasonable number of variables and keep computation relatively fast in the higher dimensional cases.

With these two equations, we are able to define a single vector which will describe the displacements, active stress, pressure and recovery of the entire system at any point in time. We call this vector our state vector, and we describe how we will utilize the Kalman Filter to improve our calculations in the following section. Our state vector is set up as follows:

$$ec{\xi} = egin{bmatrix} ec{T}^{active} \ ec{w} \ ec{\delta x} \end{bmatrix}$$

# 2.3 The Kalman Filter

The Kalman Filter (KF) is one data assimilation technique that allows us to reconstruct estimates of our state vector  $\xi_j$ , which is an estimate of the entire state at time j, from a measurement of some subset of the state. In general, these measurements will not be perfect and will have some associated error. At this time, we approximate this noise with a normal random variable with mean 0 and known measurement error covariance R. We also assume that this noise is additive, and that we can measure the system at every time step. This final assumption does not generally need to be true, but we utilize it at this time. Additionally, we know our dynamical model to not be entirely physically realistic. We assume that our uncertainty can also be approximated with a zero mean normal random variable, this time with model error covariance Q. Generally, we will not know the value of Q, but it can be roughly estimated. Additionally, we will generally not know the value of R, but this can also be estimated via measurements of known real-world quantities. In our case, the model being used for predictions will perfectly match the model which generated the data, but we will still provide a nonzero covariance, Q to represent general uncertainty for the model, including uncertainties in the initial conditions, which can lead to divergence in systems exhibiting chaotic dynamics.

With knowledge of a dynamical model that roughly describes our system, as well as measurements of some variable of interest in the system, we are able to proceed with applying the KF to improve our estimates of the behavior of the system. In doing so, we also construct running estimates of the error associated with our estimation in the form of a covariance matrix,  $P_j$ . For the standard KF, we assume that our system is linear and propagates with some linear dynamics represented by the matrix  $F_j$ . To begin, we first calculate our *prediction* 

or background step. That is, we apply our dynamical model to our most recent estimate of the state to propagate our estimate forward in time:

$$\hat{\xi}_{j|j-1} = F_j \hat{\xi}_{j-1|j-1}$$

$$P_{j|j-1} = F_j P_{j-1|j-1} F_j^T + Q$$
(5)

$$P_{j|j-1} = F_j P_{j-1|j-1} F_j^T + Q (6)$$

After that, we compare a measurement of our system to our new estimate. First, we calculate our innovation,  $\hat{y}_i$  by subtracting our measured value  $y_i$  from what we expect to measure. We create our expected measurement by applying a linear transformation,  $H_j$ , which represents our measurement scheme. Using these values, we can then estimate our innovation covariance,  $S_j$  and from this value our Kalman gain,  $L_j$ :

$$\hat{y}_j = y_j - H_j \hat{\xi}_{j|j-1} \tag{7}$$

$$S_j = H_j P_{j|j-1} H_j^T + R (8)$$

$$L_j = P_{j|j-1} H_i^T S_i^{-1} (9)$$

This Kalman gain matrix is optimal if our model perfectly matches the real system, the noise entering the system is known to be white, and if we know the covariance matrices, Q and R, exactly.<sup>20</sup> With our innovation and gain matrix, we are then able to complete our update or analysis step and create our newest, most up-to-date estimates of our entire state space, even if we only measure a subset of the state space:

$$\hat{\xi}_{j|j} = \hat{\xi}_{j|j-1} + L_j \hat{y}_j$$

$$P_{j|j} = (I - L_j H_j) P_{j|j-1}$$
(10)

$$P_{j|j} = (I - L_j H_j) P_{j|j-1} \tag{11}$$

This Kalman gain is chosen such that we minimize the expected value of the error norm,  $E[||e_j||^2|y_0, y_1, ..., y_{j-1}]$ , that is, the expected error at time j is minimized, given knowledge of all previous j-1 measurements. The Kalman Filter will run and should function properly as long as the measured subset of the state space consists of an observable subspace of the state space.

At this time, we could attempt to utilize the standard KF along with a linear approximation of our dynamical system, that is the Otani et al. system and the FHN model, which requires us to assume that our error distributions also undergo a simple linear transformation and remain normal. However, the FHN model is nonlinear and so we can not assume that our posterior distributions will remain a linear transformation of the original distributions, especially around the sharp depolarization and repolarization curves. For this reason, we will instead utilize a nonlinear filter to attempt to better utilize all of the information we get from the nonlinear model.

# 2.4 The Unscented Kalman Filter

The Unscented Kalman Filter (UKF) works with the two steps presented earlier, the prediction step and the update step. However, the UKF is capable of handling nonlinear functions for both the model equations, F and the measurement scheme, H. In doing so, the UKF utilizes much more complicated mathematics and equations, so the processes utilized by the UKF algorithm will only be described here in brief. To begin, the UKF relies on the Unscented Transform (UT), which deterministically generates a minimal set of 'sigma' points to act as samples of the state space. For an n-dimensional state space, we will construct 2n+1 sigma points which are each n-dimensional. Each of these points has associated weights. The construction of these sigma points rapidly becomes expensive as n increases, as the construction relies on the calculation of matrix square roots of larger and larger matrices. Each of these 2n+1 sigma points is then propagated through the nonlinear model, and combined with the weights to construct an average, which constitutes our new predicted estimate of the state space and error covariance.

To calculate our update/analysis step, we then construct a second set of 2n + 1 sigma points around our predicted estimate and propagate these values through a nonlinear measurement scheme. Combining these estimates with our measurements allows us to calculate our new innovation, a cross covariance matrix and finally our optimal Kalman gain. This Kalman Gain is then applied in much the same way as in the linear filter to produce our most up-to-date estimates of the system. This entire process is highly computationally complex and, for larger systems, becomes computationally infeasible.

For our problem, we are simulating measurements of our displacements,  $\delta \vec{x}$ , and using this to construct and improve estimates of our voltages  $\vec{v}$ ; we assume that these variables constitute an observable subspace for all time. We are using n=100 nodes in a cable geometry, Euler time step size  $\Delta t=0.01$ , and spatial discretization size  $\Delta x=0.25$ . We first generate AP propagation data using the FHN model from time t=0 to time t=20. From this data, we solve the forward problem at every time step to calculate the true displacement of every node. From these displacements, we add normally distributed random noise with mean 0 and known covariance to simulate measurement uncertainty. At this point, we utilize MATLAB's mldivide function to directly solve the inverse problem to ill effect. We then use MATLAB's built-in unscentedkalmanfilter function to attempt to reconstruct the unmeasured membrane potentials.

#### 3. RESULTS

Figure 1a shows the propagation of the APs through time as a wave of higher voltage passing from left to right. From this information we construct the data in Figure 1b by solving the forward problem, which gives us the displacement data we will use for the remainder of our results. The solution to the inverse problem, shown in Figure 1c, from this data differs only minimally from Figure 1a, hence suggesting we were able to accurately reconstruct the original active stress wave. In Figure 1d, we have added noise to the displacements shown in 1b that corresponds to roughly 10% error in our measurements. Comparing Figure 1d to Figure 1b, we can see that the two figures are nearly identical and the noise is mostly insubstantial.

We can now discuss and compare the results of our two estimation schemes. Firstly, in Figure 1e, we see our naive least-squares solution to the inverse problem. Note that the solution has almost entirely degraded and the AP is obscured heavily by the noise. Also of note is the scale of this solution, which is nearly twenty times the scale from Figure 1a. This suggests that our AP data has been nearly entirely lost to noise. Next we compare this result to the result shown in Figure 1f, which shows our UKF estimated solution to the inverse problem. Compared to Figure 1a we can see that some noise artifacts still remain in our solution, but when compared to Figure 1e, the improvement we see is very significant. Our AP has been clearly resolved and the scale has greatly improved over the scale seen in the least-squares solution. The only area where the UKF shows any real issues is around approximately time t=0, where we see that the unknown initial state results in some transient behavior which quickly decays as we converge with the true state.

Inspecting Figure 1g, we see the residual deviation of the least-squares solution to the inverse problem. Note that areas colored white represent areas where our estimated solution is close to the actual solution. With that in mind, it is clear from this figure that we have a large number of points with large deviations from the actual membrane potential, thus illustrating the poor job our least-squares solution does at solving this inverse problem when noise is present.

This is in comparison to Figure 1h, where we see the residual deviation of the UKF estimate solution to the inverse problem. We next compare the residual error following the direct active stress reconstruction 1g to the residual error following the UKF reconstruction 1h. The difference between Figure 1g and Figure 1g is quite stark. Nearly all of the residual deviation from the UKF is of order unity, while the residual deviation for the least-squares solution has a number of points that are of order 10, suggesting that our UKF solution is an order of magnitude more accurate than our least-squares solution. This confirms the qualitative difference we observed between Figures 1e and 1f.

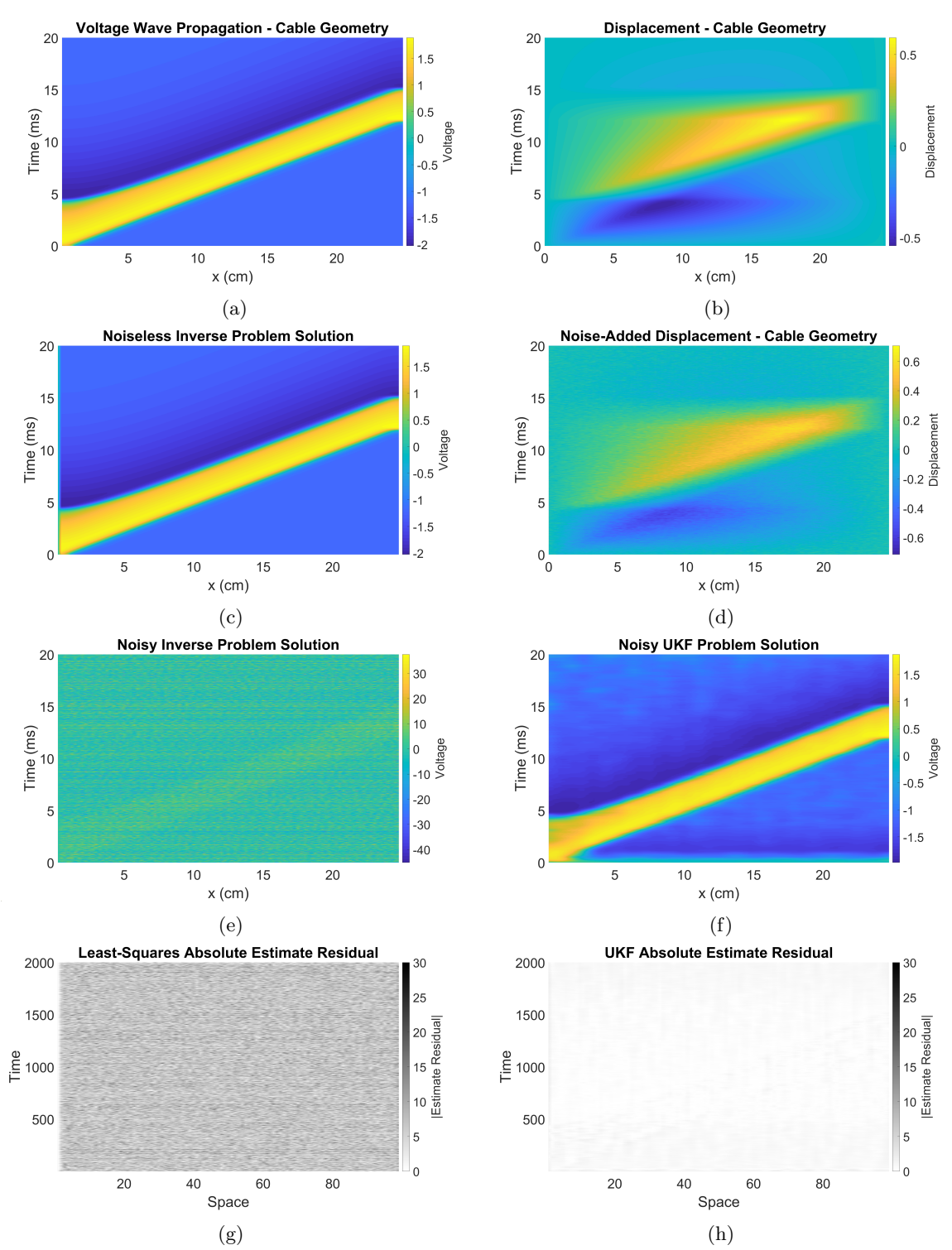


Figure 1: a shows the propagation of APs along the cable from left-to-right, and b shows the displacement in response to the changes in the APs. c shows the least-squares solution to the inverse problem in the absence of noise. d shows the displacements from b with around 10% random noise added. e shows our least-squares inverse problem solution with the added noise, while f shows our UKF estimate solution. Figures g and h show the difference between our estimated solutions and the actual solutions to the inverse problem, for Least-Squares and the UKF, respectively.

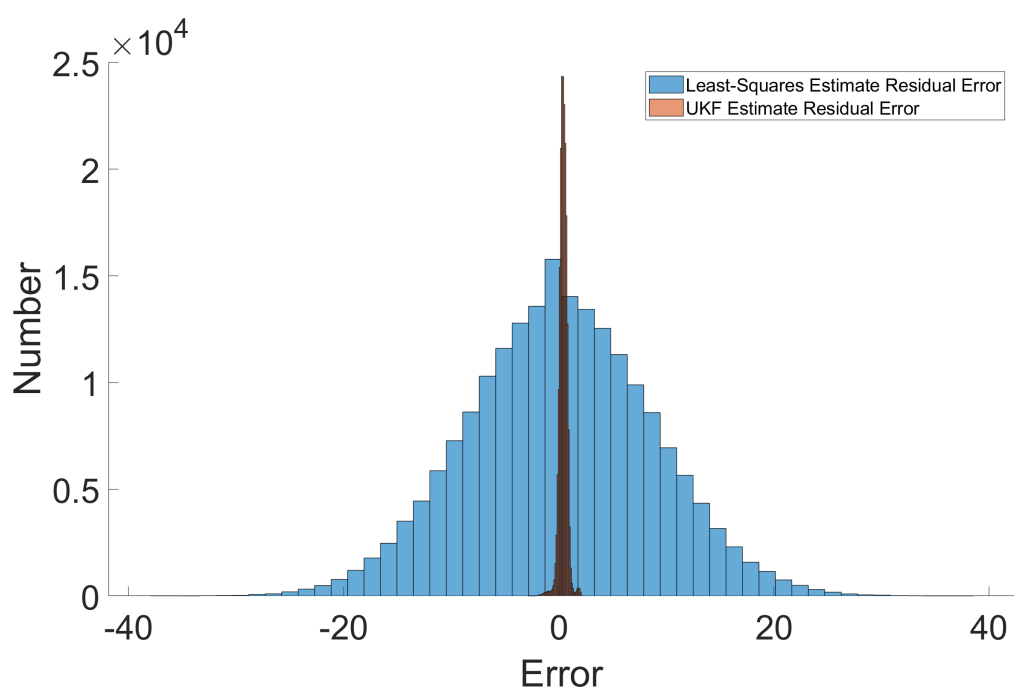


Figure 2: A histogram showing the distribution of errors associated with the Least-Squares estimate error and the UKF estimate error. Note that both histograms suggest a roughly normal distribution of the error associated with each method.

In Figure 2, we show a pair of histograms to compare the distribution of the errors seen in Figures 1g and 1h. Both histograms suggest a normal distribution, though the parameters associated with each of these distributions varies widely. The Least-Squares approximation has a mean residual error of 0.1115 and a residual error variance of 72.4079, while the UKF approximation has a mean residual error of 0.4127 and a residual error variance of 0.1295. This suggests that the UKF may have a slight tendency to overestimate the membrane potentials but its predictions are highly precise. And while the Least-squares approximation may have a smaller mean residual error, the fact that the error variance associated with this method is so high means that its reconstruction is highly unreliable.

## 4. CONCLUSIONS AND FUTURE WORK

In this work we are describing the first implementation and demonstration of a novel method for estimating the propagation of action potentials in cardiac tissue from noisy measurements of tissue motion. This method utilizes the Unscented Kalman Filter to track our error-prone measurements in conjunction with the Otani et al. and FitzHugh-Nagumo models to define how the action potential wave should propagate and generate the active stresses, which in turn generate fiber contractions. Here we demonstrate an implementation of the proposed method in cable geometry that mimics the behavior of cardiac fibers when AP wave propagation is present, and shows improved results compared to those we have reported previously in Otani et al.

The UKF is used to improve our estimates of active stresses in the cardiac muscle which induce the measured deformation of the cardiac tissue. Our results significantly improve on the previous results and provide a way to move forward in the larger project, but have thus far only been completed in the 1-dimensional case. Preliminary testing has begun on a 3-dimensional version of the UKF estimations of the problem, but the intense computational complexity has made this work rather difficult and quite slow, even in a relatively small domain. While the UKF delivers reasonably good results, we anticipate that as we move to more complex scenarios we will in turn require more points in space to adequately represent the chaotic dynamics we wish to investigate. As such, we are also investigating an implementation of the Ensemble Transform Kalman Filter and the Local Ensemble Transform Kalman Filter. We believe that these filters should provide comparable results while allowing us to

more quickly compute these results, even in much larger regimes. This will allow us to investigate the usage of our techniques to examine more complex dynamics such as spiral or scroll waves or more chaotic scenarios corresponding to fibrillation. Additional statistical analysis is required to further verify our results and we will look to compare our UKF results with those associated with other smoothing and regularization methods.

#### **ACKNOWLEDGMENTS**

This work has been supported in part by the Computing & Data-enabled Science and Engineering Award No. 1808530 from the Office of Advanced Cyberinfrastructure of the National Science Foundation.

#### REFERENCES

- Sampson, K. J. and Henriquez, C. S., "Simulation and prediction of functional block in the presence of structural and ionic heterogeneity," *American Journal of Physiology-Heart and Circulatory Physiology* 281, H2597–H2603 (Dec. 2001).
- [2] Ramanathan, C., Ghanem, R. N., Jia, P., Ryu, K., and Rudy, Y., "Noninvasive electrocardiographic imaging for cardiac electrophysiology and arrhythmia," *Nature Medicine* **10**, 422–428 (Apr. 2004).
- [3] Wang, Y. and Rudy, Y., "Application of the Method of Fundamental Solutions to Potential-based Inverse Electrocardiography," *Annals of Biomedical Engineering* **34**, 1272–1288 (Aug. 2006).
- [4] El-Sherif, N., Chinushi, M., Caref, E. B., and Restivo, M., "Electrophysiological mechanism of the characteristic electrocardiographic morphology of torsade de pointes tachyarrhythmias in the long-QT syndrome: detailed analysis of ventricular tridimensional activation patterns," *Circulation* **96**(12), 4392–4399 (1997).
- [5] Frazier, D. W., Wolf, P. D., Wharton, J. M., Tang, A. S., Smith, W. M., and Ideker, R. E., "Stimulus-induced critical point. Mechanism for electrical initiation of reentry in normal canine myocardium.," The Journal of Clinical Investigation 83, 1039–1052 (Mar. 1989).
- [6] Pogwizd, S. M. and Corr, P. B., "Reentrant and nonreentrant mechanisms contribute to arrhythmogenesis during early myocardial ischemia: results using three-dimensional mapping.," *Circulation research* **61**(3), 352–371 (1987).
- [7] Langrill Beaudoin, D. and Roth, B. J., "Effect of plunge electrodes in active cardiac tissue with curving fibers," *Heart Rhythm* 1, 476–481 (Oct. 2004).
- [8] Baxter, W. T., Mironov, S. F., Zaitsev, A. V., Jalife, J., and Pertsov, A. M., "Visualizing Excitation Waves inside Cardiac Muscle Using Transillumination," *Biophysical Journal* 80, 516–530 (Jan. 2001).
- [9] Hillman, E. M. C., Bernus, O., Pease, E., Bouchard, M. B., and Pertsov, A., "Depth-resolved optical imaging of transmural electrical propagation in perfused heart," *Optics Express* **15**, 17827–17841 (Dec. 2007).
- [10] Wellner, M., Bernus, O., Mironov, S. F., and Pertsov, A. M., "Multiplicative optical tomography of cardiac electrical activity," *Physics in Medicine and Biology* **51**, 4429–4446 (Aug. 2006).
- [11] Otani, N. F., Luther, S., Singh, R., and Gilmour, R. F., "Transmural Ultrasound-based Visualization of Patterns of Action Potential Wave Propagation in Cardiac Tissue," *Annals of Biomedical Engineering* 38, 3112–3123 (Oct. 2010).
- [12] Pernot, M., Fujikura, K., Fung-Kee-Fung, S. D., and Konofagou, E. E., "ECG-gated, Mechanical and Electromechanical Wave Imaging of Cardiovascular Tissues In Vivo," *Ultrasound in Medicine & Biology* 33, 1075–1085 (July 2007).
- [13] Wang, S., Lee, W., Provost, J., Luo, J., and Konofagou, E. E., "A composite high-frame-rate system for clinical cardiovascular imaging," *IEEE Transactions on Ultrasonics, Ferroelectrics, and Frequency Control* 55, 2221–2233 (Oct. 2008).
- [14] Wang, L., Zhang, H., Wong, K. C. L., Liu, H., and Shi, P., "Physiological-Model-Constrained Noninvasive Reconstruction of Volumetric Myocardial Transmembrane Potentials," *IEEE Transactions on Biomedical Engineering* 57, 296–315 (Feb. 2010).
- [15] Julier, S. J. and Uhlmann, J. K., "New extension of the Kalman filter to nonlinear systems," in [Signal Processing, Sensor Fusion, and Target Recognition VI], 3068, 182–193, International Society for Optics and Photonics (July 1997).

- [16] Julier, S. J. and Uhlmann, J. K., "Unscented filtering and nonlinear estimation," *Proceedings of the IEEE* 92, 401–422 (Mar. 2004).
- [17] Wan, E. A. and Merwe, R. V. D., "The unscented Kalman filter for nonlinear estimation," in [Proceedings of the IEEE 2000 Adaptive Systems for Signal Processing, Communications, and Control Symposium (Cat. No.00EX373)], 153–158 (Oct. 2000).
- [18] FitzHugh, R., "Impulses and Physiological States in Theoretical Models of Nerve Membrane," *Biophysical Journal* 1, 445–466 (July 1961).
- [19] Izhikevich, E. M. and FitzHugh, R., "FitzHugh-Nagumo Model," Scholarpedia 1, 1349 (Sept. 2006).
- [20] Kalman, R. E., "A new approach to linear filtering and prediction problems," *Journal of Basic Engineering* 82(1), 35–45 (1960).